

Citation for published version:
Zhao, H, Xiang, Y, Shen, Y, Guo, Y, Xue, P, Sun, W, Cai, H, Gu, C & Liu, J 2022, 'Resilience Assessment of Hydrogen Integrated Energy System for Airport Electrification', *IEEE Transactions on Industry Applications*, vol. 58, no. 2, pp. 2812 - 2824. https://doi.org/10.1109/TIA.2021.3127481

DOI:

10.1109/TIA.2021.3127481

Publication date: 2022

Document Version Peer reviewed version

Link to publication

© 2021 IEEE. Personal use of this material is permitted. Permission from IEEE must be obtained for all other users, including reprinting/ republishing this material for advertising or promotional purposes, creating new collective works for resale or redistribution to servers or lists, or reuse of any copyrighted components of this work in other works.

# **University of Bath**

# **Alternative formats**

If you require this document in an alternative format, please contact: openaccess@bath.ac.uk

Copyright and moral rights for the publications made accessible in the public portal are retained by the authors and/or other copyright owners and it is a condition of accessing publications that users recognise and abide by the legal requirements associated with these rights.

Take down policy
If you believe that this document breaches copyright please contact us providing details, and we will remove access to the work immediately and investigate your claim.

Download date: 07 Mar 2023

# Resilience Assessment of Hydrogen Integrated Energy System for Airport Electrification

Huangjiang Zhao, Yue Xiang, Senior Member, IEEE, Yichen Shen, Yongtao Guo, Ping Xue, Wei Sun, Member, IEEE, Hanhu Cai, Chenghong Gu, Member, IEEE, Junyong Liu, Member, IEEE

Abstract—In recent years, the idea of green aviation and environmental protection has received increasing attention from the aviation industry. Hydrogen energy has an important role in the transition to low-carbon energy systems. To address that, this paper conducts the techno-economic analysis for the hydrogen energy system, photovoltaic energy (PV), battery storage system (BSS), electric auxiliary power unit (APU) of aircraft, and electric vehicles (EVs) into the electrified airport energy system. Specifically, the model quantifies aircraft electrical load based on passenger' travel behavior, establishes a corresponding APU load characteristic model, and establishes an EV charging load profile based on the flight schedule and sequencing algorithm. A mixed-integer linear programming (MILP) optimization method based on life cycle theory was proposed, to minimize the total costs of hydrogen integrated energy systems for airports (HIES). However, the resilience advantages of hydrogen energy concerning power failure are little explored in existing academic research. Thus, a resilience assessment method and improvement measure were proposed for HIES. Case studies have been conducted under different optimal hydrogen energy integration configurations and disaster times with resilience assessment by considering periods when the power supply capacity of the grid is insufficient. The results show the effectiveness of the proposed method.

*Index Terms*—Hydrogen integrated energy system (HIES), airport electrification, techno-economic analysis, electric vehicle, resilience assessment, enhancement strategy.

#### Nomenclature

| $m_t^{out,H_2}, m_t^{out,O_2}$   | amounts of hydrogen and oxygen produced by electrolyzer at time slot <i>t</i> (kg/hr) |
|----------------------------------|---|
| $P_t^{in,electrolyzer}$          | input power of electrolytic   |
| $P_t^{FC}$                       | output of fuel cell at time slot $t$  |
| $m_{t+1,H_2}^s$ , $m_{t,H_2}^s$  | storage capacity of hydrogen at time slots $t+1$ and $t$                              |
| $P_{t,pv}^{out}$                 | output power of PV at time slot $t$   |
| $E_{t+1}^{BSS}$ , $E_t^{BSS}$    | energy stored at time slots $t+1$ and $t$   |
| $P_t^{in,BSS}$ , $P_t^{out,BSS}$ | charging and discharging power of BSS   |

This work was supported by the National Natural Science Foundation of China (U2166211). (Corresponding author: *Yue Xiang.*)

Huangjiang Zhao, Y. Xiang, Yongtao Guo, Ping Xue, Junyong Liu are with College of Electrical Engineering, Sichuan University, Chengdu 610065 China (e-mail: zhaohuangjiang@stu.scu.edu.cn; xiang@scu.edu.cn; yongtao\_guo@outlook.com; xpsherry@foxmail.com; liujy@scu.edu.cn).

| P <sup>aircrafts</sup> <sub>t,conract stands</sub> | at contact stands at time slot $t$                                     |
|--|--|
| $P_{t,remote\ stands}^{aircrafts}$                 | electric APU load demand of aircraft at remote stands at time slot $t$ |
| $P_t^{grid,buy}$                                   | grid power purchased time slot $t$ (kW)                                |
| $P_{month}^{demand,	ext{max}}$                     | maximum power demand per month (kW)                                    |
| $P_t^{pv}$   | PV power consumed of PV at time slot t                                 |
| $P_t^{EVs}$  | load of EVs at time slot $t$   |
| $\lambda^{shortage,H_2}$                           | proportion of hydrogen shortage  |
| $R_{lpha}\left(T ight)$                            | resilience assessment index for airport energy system                  |
| R(T)   | comprehensive resilience index for airport energy system               |

electric APU load demand of aircraft

#### I. INTRODUCTION

C arbon emissions in the field of transportation account for approximately 30% of the total economic and social carbon emissions [1]. Therefore, energy conservation and emission reduction in the transportation sector are of great significance to achieve the ambitious decarbonization goals around the world. In addition, compared to road and rail transportation, the aviation industry still mostly depends on fossil fuels, indicating the urgency and complexity of aviation decarbonization. Electrification is a promising approach to achieve the low-carbon aviation goals, and this method has also been considered by many airlines and manufacturers to transit to electric aircraft and hybrid-electric aircraft [2]. However, electric aircraft experiences many technical challenges, high costs, and poor weather adaptability. Therefore, this article focuses on the early feasible realization of the electrification of ground service equipment in airports as mainly reflected in the two following aspects: i) Ground vehicles in the airport, including passenger shuttle bus, aircraft tractors, aircraft guided vehicles, service vehicles, freight trailers, and forklifts are fully electrified; ii) Ground power unit is used to power the aircraft when the aircraft is on the

Yichen Shen, Chenghong Gu are with the Department of Electronic & Electrical Engineering, University of Bath, Bath, UK.(email: Y.Shen@bath.ac.uk; C.Gu@bath.ac.uk).

Wei Sun is with the School of Engineering, University of Edinburgh, EH93DW Edinburgh, U.K (e-mail: w.sun@ed.ac.uk).

Hanhu Cai is Southwest Electric Power Design Institute CO., LTD. of China Power Engineering Consulting Group, Chengdu, China (e-mail: caihanhu@swepdi.com).

ground, instead of using the auxiliary power unit(APU) onboard, known as the APU alternative state.

Photovoltaic power generation systems and battery energy storage systems have been used in some airport energy systems. The large areas of the airport, including the airport terminal roof, open space, and green belt, provide good land availability to develop photovoltaic (PV) power generation. PVs provide a clean power supply but suffer the issue of intermittency [3]. Battery energy storage (BSS) systems can help reduce the variability of PV output but have a short life cycle and high replacement costs. Hydrogen energy is a wellrecognized clean energy source, with the advantages of high energy density, high application efficiency, multiple source channels, and convenient transportation [4]. The hydrogen energy system consists of three parts, namely, the electrolyzer, fuel cell, and hydrogen storage tan [5], which together can provide a sustainable and flexible energy supply. The fuel cell power generation in the hydrogen energy system provides great flexibility for the power supply of the aircraft APU at airport remote stands and reduces the emission pollution and noise caused by traditional fuel-powered APU. In comparison with PV and BSS, the integration of hydrogen energy systems can effectively alleviate their shortcomings. Carbon emission can be mitigated by employing the electrification of airport energy systems within hydrogen resource deployment to supply airport and airport load in the future. Thus, based on the hydrogen energy system, PV, BSS, electric APU of aircraft, and electric vehicles (EVs), an energy system with high penetration of hydrogen resources for the airport is modeled in this paper.

In recent years, large-scale power outages caused by extreme events occurred repeatedly at home and abroad [6]. To deal with the blackout accident caused by extreme events with small probability and the high impact such as natural disasters and cascading failure, the concept of power system resilience was created. Resilient power grid refers to the ability to comprehensively, quickly, and accurately sense the operation situation of the grid, coordinate with internal and external resources of the grid, actively predict and prepare for various disturbances, actively defend, quickly restore important power loads, and learn from and continuously improve itself [7]. The microgrid can be used in the data center, modern building, airport, and industrial park to improve the efficiency and reliability of the power supply and improve the power quality of users [8]. The energy system of the airport is a typical microgrid system. Extreme events such as severe weather, natural disaster, and unplanned island caused by physical and cyber attacks pose a serious threat to system operation [9]. In addition, with the access of the high proportion of clean energy and electric vehicles, random and fluctuating clean energy output and uncertain load shock, and other small-signal events will also bring challenges to the stability control of microgrid.

Resilience research on microgrids mainly focus on two aspects: (1) As a resilient resource, a microgrid can improve the resilience of a large grid by using a local power generation system under the worst situations [9,10]; (2) Improve the survivability of important loads in the microgrid. Some studies have been done to enhance the resilience of the system by

using power electronics equipment [11], improved control strategies [12], and resistance to network attacks [9]. As a critical infrastructure in our society, the energy supply system in airports should be able to maintain operation under various disturbances including extreme events. However, the low probability high impact events, such as airport blackout are more likely to be triggered with the high proportion renewable in the integrated energy system. Thus, with the increasing decarbonization of airport energy systems, more concerns should be also turned to enhance their operational safety and resilience. Airport energy system resilience refers to the ability of the airport energy system to rapidly adjust its energy supply and quickly return to the normal state of energy supply when the airport encounters an unexpected drop of power supply from the main network. The resilience of airport energy systems is the deep coupling of multiple energy subsystems.

Most of the previous studies have implemented a multiobjective optimization model for optimal sizing and dispatching of microgrids disregarding while ignoring the elasticity value. They have mainly focused on technoeconomic-environmental performance enhancement of microgrids from demand response [13,14], load flexibility [15,16], minimum capital and operating cost [17-19], maximum use of renewables, and reduced greenhouse gas emission [18,19]. Little work has been done to quantify the grid-connected microgrids' resilience value, especially during power grid disruption. Reference [20] proposed an optimization model that shows the value of lost load and battery price to quantify and monetize the resilience value. Zhou et al. adopted the same approach focusing on the importance of battery capacity and price on system cost and reduces the probability of load loss [17]. However, in both cases, the blackout accident is ignored. A techno-economic optimization model comprising PV and Battery for different commercial buildings in three cities has been presented in [21], the cost of the islanded microgrid and the sensitivity of outage costs have been extensively discussed. Rosales et al. designed a method to quantify the benefits from both business-related and energy resilience perspectives provided by a microgrid based on PV and electrochemical energy storage integrated into large buildings [22]. however, they did not discuss the enhancement strategy of the microgrid in case of the blackout accident of the power grid. Anderson in [23] presented a method to quantify the amount and value of resiliency provided by renewable energy hybrid systems, which survives the blackout with a substantial economic benefit but did not describe the dispatch strategy and sensitivity in various scenarios. It is the same for the proposed demonstration project by literature [13] although they considered demand response as mentioned earlier. Therefore, although the resilience of the power system has been widely studied, the resilience of the airport energy system has not been explored yet. The ability of airport energy systems to resist threats should be understood and measured to achieve normal operation when encountering extreme disturbances.

The problems mentioned above are attempted to be addressed by proposing a resilience assessment method and proposing an improvement measure for a hydrogen integrated energy system (HIES). First, the paper establishes the model

of HIES, consisting of the hydrogen energy system, photovoltaic energy (PV), battery storage system (BSS), electric auxiliary power unit (APU) of aircraft, and electric vehicles (EVs). Based on the passenger travel behavior, an airport APU load characteristic model is established to quantify aircraft electrical requirements and establishes an EV charging profile based on the flight schedule and sequencing algorithm. Second, a mixed-integer linear programming (MILP) optimization method based on life cycle theory was proposed to design the capacity of each energy source, which aims at minimizing the total cost of HIES. Then, a resilience assessment method and improvement measure were proposed for HIES. Finally, case studies have been conducted under different hydrogen energy integration scenarios and disaster times with resilience assessment by considering periods when the power supply capacity of the grid is insufficient. The proposed method provides a comprehensive resilience assessment and enhancement strategy for different HIES scenarios. The main contributions of this article are as follows.

- An APU load characteristic model is deployed to quantify aircraft electricity load based on the flight schedules. A modeling method that generates EV charging profiles is proposed based on flight schedule and sequencing algorithm.
- 2) The paper proposes a mixed-integer linear programming (MILP) optimization method is developed to design the capacity of the hydrogen energy system, PV, and BSS based on life cycle theory, which aims at minimizing the total costs under the life cycle of the airport project.
- 3) This work innovatively proposes a resilience assessment method for the airport energy system with frequent varying flights, and a realistic flight schedule of an airport

- was applied to evaluates the proposed method. Subsequently, the resilience results of different energy configuration schemes are discussed.
- 4) An enhancement strategy is proposed based on regulating the penetration of hydrogen energy in HIES.

The rest of the paper is organized as follows. Section II provides a short description of the airport energy system framework, and in Section III, the resilience modeling approach for the airport energy system is presented. Test studies are presented in Section IV, and conclusions are drawn in Section V.

#### II. RESEARCH FRAMEWORK

This work mainly focuses on the energy system outside the airport terminals. The energy supply targets are mainly aircraft and EVs. Generally, passengers will be arranged for different boarding methods based on the location of the aircraft. Passengers of the aircraft parked in contact stands can board the plane through the boarding bridge, while aircraft parked in remote stands need to take the shuttle bus to the aircraft dock to board the plane. It is assumed that there is a power supply installed under each boarding bridge at contact stands to supply power for the aircraft. Some airports have power distribution boxes at the apron, which need to be connected to the power car through a long-distance intermediate power cable [24]. However, the majority of airports still use onboard APU to supply aircraft at remote stands. In addition, electric vehicles at the airport are increasingly used to replace traditional fuel vehicles.

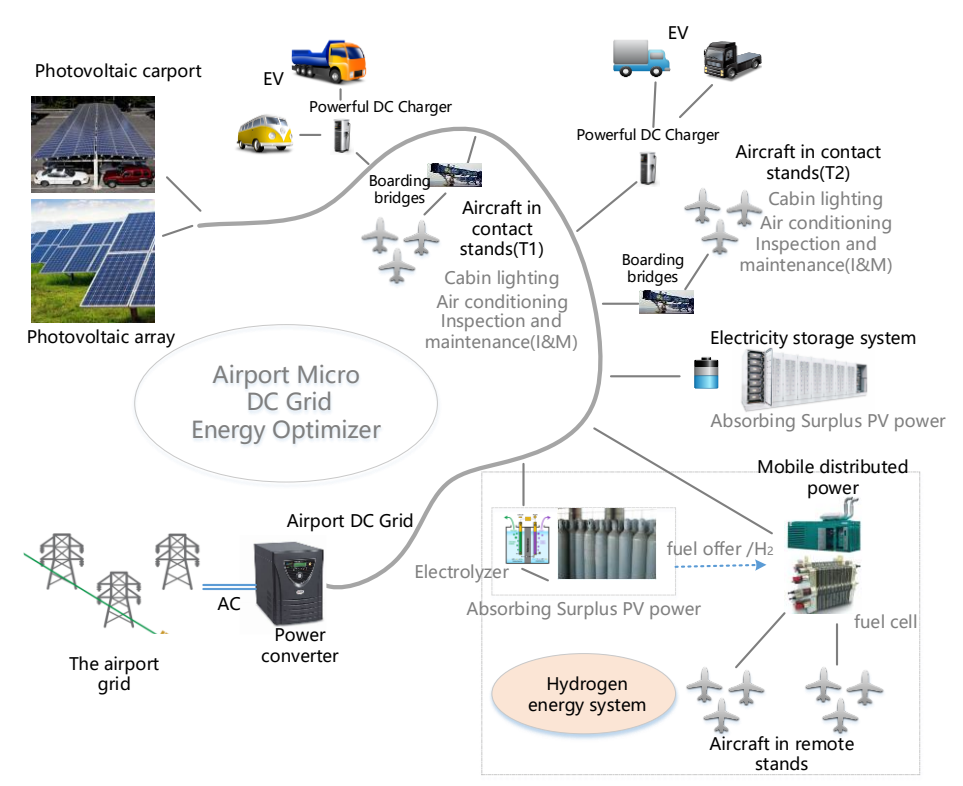


Fig. 1. Structure of HIES based on the integrated energy system

The structure of HIES based on the integrated energy system is shown in Figure. 1. This paper proposes an airport energy supply structure based on the integrated energy system to study the energy system outside the airport terminal, including the main grid, hydrogen energy system, PV, BSS, and EVs. This system integrates multiple energy sources with different energy carriers through converters, energy distribution, and storage components in an optimal manner for various airport energy use. The electrolyzer and the supporting hydrogen storage tank provide hydrogen production and storage respectively. The fuel cell in the hydrogen energy

system is designed as a mobile power source and mounted on the ground vehicle, and this structure can supply power to the aircraft APU at a remote stand and also be connected to the integrated energy system to provide energy for the entire airport energy system. The hydrogen energy system, PV, BSS, EVs, and electric loads can exchange energy by autonomous distributed control systems based on the DC voltage. In this paper, the operating voltage of the DC microgrid was set to 600 V, which can be directly connected with BSS. The voltage of the 600 V DC grid was reduced to the output voltage required by loads (380 V/400 V).

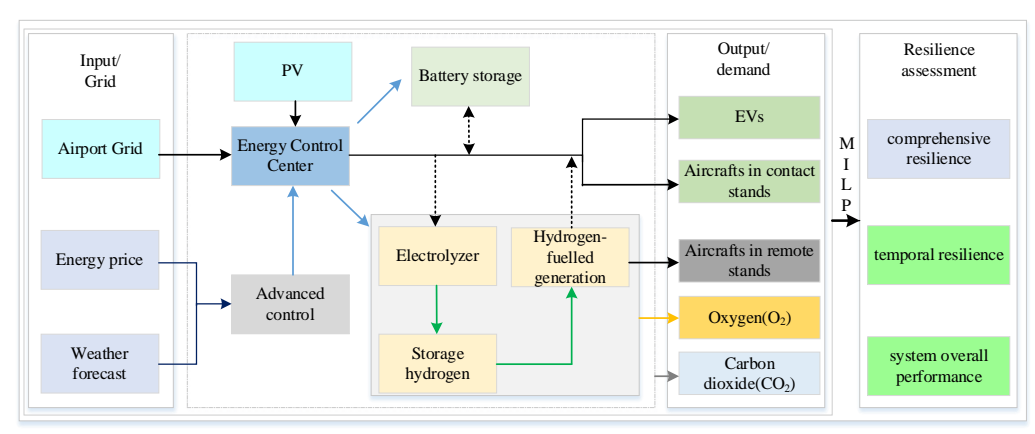


Fig. 2. Overall framework

Additional new energy sources are applied in the airport to improve the overall performance of energy supply and reducing carbon emissions of the aviation industry by promoting the development of the electrified airport. Solar energy is the form of renewable energy considered in this work, where the PV can be installed on the roof of the terminal and open space in the apron. The PV energy is used to power the electrical facilities in both the airside and landside of the airport (aircraft electric APU, EVs electric demand) [25]. Considering that PV power generation is restricted by weather factors, this paper proposes a hydrogen-solar-storage integrated microgrid design to balance the renewable supply with demand. The excess electrical power is converted to hydrogen and oxygen using the electrolysis in HIES. The produced green hydrogen is stored in a hydrogen tank and provides energy for the airport at remote stands through fuel cell power generation when it is needed. The produced oxygen can be also used as additional financial income. All the distributed energy supply and demand are connected and managed together via a microgrid system by an energy control center. The operation of HIES is optimized by the MILP model, to minimize the total annual cost of HIES while configuring the capacity of various energy devices for the airport, and finally evaluate the resilience of HIES. The overall framework is presented in Figure. 2. In section III, the detailed energy system modeling is presented.

### III. A MODELING APPROACH FOR AIRPORT ENERGY SYSTEM RESILIENCE

- A. Hydrogen integrated energy system
- 1) Hydrogen energy system model

The hydrogen energy system model can provide a sustainable and flexible power source for the renewable energy system. The hydrogen energy system consists of three parts, namely, the electrolyzer, fuel cell, and hydrogen storage tank. When the photovoltaic resources are in excess, the electrolyzer uses surplus solar energy to split water to produce hydrogen, which is then stored in the hydrogen storage tank. When the PV resources are insufficient, the fuel cell uses the stored hydrogen as fuel to generate electricity to meet the demand of the electric load. The fuel cell considered here is the proton exchange membrane fuel cell, which uses hydrogen and oxygen as fuel to convert chemical energy into electrical energy for storage. The hydrogen fuel cell is pollution-free, noise-free, and highly efficient. The fuel cell power generation is designed by combining multiple small fuel cell units as a whole that can meet the maximum load at remote stands [25]. Hydrogen storage tanks are used to store hydrogen produced via the electrolysis of water and can provide hydrogen for fuel cells, thus increasing the flexibility of the system to improve its flexibility. Equations (1), (2), (3) and (4) [26,27] provide expressions for the electrolyzer, fuel cell, and hydrogen storage tank, respectively:

$$m_t^{out, H_2} = \frac{3.6 P_t^{in, electrolyzer} \Delta t}{h_{\text{HHV}}^{H_2}} \eta^{electrolyzer}$$

$$m_t^{out, O_2} = 8 m_t^{out, H_2}$$

$$P_t^{FC} = a + b F_t^{H_2}$$
(3)

$$m_t^{out,O_2} = 8m_t^{out,H_2}$$
 (2)

$$P_t^{FC} = a + b F_t^{H_2} \tag{3}$$

$$P_{t}^{s} = a + b F_{t}^{s}$$

$$m_{t+1,H_{2}}^{s} = m_{t,H_{2}}^{s} + \left(m_{t,H_{2}}^{s,in} - m_{t,H_{2}}^{s,out}\right) \Delta t$$
(4)

where  $h_{\scriptscriptstyle \mathrm{HHV}}^{\scriptscriptstyle H_2}$  denotes the heating value of hydrogen,  $\eta^{\scriptscriptstyle electrolyzer}$ 

denotes the efficiency of electrolyzer(MJ/kg), and  $F_t^{H_2}$  denotes the hydrogen consumption rate,  $P_t^{FC}$  denotes the output of fuel cell at time slot t (kg/hr), a and b denote the fuel cell power generation coefficients,  $m_{t,H_2}^{s,im}$  and  $m_{t,H_2}^{s,out}$  are the hydrogen charging/discharging flow(kg/hr).

#### 2) PV system model

The error can be reduced and the accuracy of the model can be improved by incorporating the actual light intensity and the ambient temperature at the same time in the actual output power of the photovoltaic cell, as shown in Equation (5) [28].

$$P_{t,pv}^{out} = N_{pv} P_{STC} \frac{I_t}{I_{STC}} [1 + \alpha (T_{t,c} - T_{c,STC})]$$
 (5)

where  $N_{pv}$  denotes the number of PV panels, STC denotes standard text conditions,  $P_{STC}$  denotes the rated power of PV panel(STC, Cell temperature 25°C, irradiance 1000 W/m2),  $I_t$  is the solar radiation intensity at time slot t,  $I_{STC}$  denotes the irradiance intensity at STC,  $\alpha$  denotes the power temperature coefficient,  $T_{t,c}$  is the PV cell temperature at time slot t, and  $T_{c.STC}$  is the PV cell temperature at STC.

# 3) BSS modeling

The battery energy storage system is used for energy arbitrage and the storage of excess PV energy. In an energy system, a BSS can be considered as a load when it charges, and as an energy source when it discharges. Li-ion batteries have a high energy density, long life, low self-discharge, fast charging, and good safety performance. Therefore, Li-ion batteries with multiple energy storage units were applied to battery storage systems in this study [25].

The battery can effectively suppress the fluctuation caused by the sudden change of the load demand of the microgrid. When the PV output power is greater than the load demand power, the battery is charging. Alternately, the battery is in a discharged state. The battery storage model is modeled in (6) [29].

$$E_{t+1}^{BSS} = (1 - \delta)E_t^{BSS} + (\eta^c P_t^{in,BSS} - P_t^{out,BSS} / \eta^d)\Delta t$$
 (6)

where  $\delta$  is the standby energy loss ratio,  $\eta^c$  and  $\eta^d$  are the charging efficiency and discharging efficiency.  $\Delta t$  is the time step.

#### 4) Electric APU load model of aircraft

The airport energy system must supply sufficient power to the airborne APU within aircraft turnaround time to meet the power demand of aircraft flight. According to the aircraft flight plan, the paper innovatively establishes an electric APU load model of aircraft to quantify the aircraft power demand.

To simplify the electrical load model of aircraft, we applied the following assumptions:

- 1) All aircraft have the same electric APU load;
- 2) The aircraft will be prioritized for parking at the contact stand. When the contact stands are full, the aircraft will park at remote stands. The electric APU load model of aircraft is indicated as follows:

$$P_{t,conract}^{aircraft} = P_{AVE}^{aircraft} \{ \min \left[ \int_{t}^{t+t^{dep}} D_{Aircraft}^{depature,T1}(t)dt + \int_{t-t^{arr}}^{t} D_{Aircraft}^{arrival,T1}(t)dt, B^{T1} \right] + \min \left[ \int_{t-t^{arr}}^{t+t^{dep}} D_{Aircraft}^{depature,T2}(t)dt + \int_{t-t^{arr}}^{t} D_{Aircraft}^{arrival,T2}(t)dt, B^{T2} \right] \}$$

$$(7)$$

$$P_{t,remode}^{aircrafts} = P_{AVE}^{aircraft} \{ \max \left[ \int_{t}^{t+t^{dep}} D_{Aircraft}^{depature,T1}(t)dt + \int_{t-t^{air}}^{t} D_{Aircraft}^{arrival,T1}(t)dt \right. \\ \left. - B^{T1}, 0 \right] + \max \left[ \int_{t}^{t+t^{dep}} D_{Aircraft}^{depature,T2}(t)dt + \int_{t-t^{air}}^{t} D_{Aircraft}^{arrival,T2}(t)dt - B^{T2}, 0 \right] \}$$

$$(8)$$

where  $P_{AVE}^{aircraft}$  denotes the average electrical power demand of aircraft,  $D_{Aircraft}^{depature,T1}(t)$  and  $D_{Aircraft}^{arrival,T1}(t)$  denote the departure/arrival flow curve function of terminal T1,  $D_{Aircraft}^{arrival,T2}(t)$  and  $D_{Aircraft}^{arrival,T2}$  denote the departure/arrival flow curve function of terminal T2.  $B^{T1}$  and  $B^{T2}$  denote the number of contact stands of T1 and T2.  $t^{dep}$  is the time consumed for the preparation for flight before departure,  $t^{arr}$  is the time consumed for the maintenance of aircraft after arrival.

# 5) EV charging load model in airport

The operation of EVs in the airport is driven by flight schedules. The paper designs a charging process for airport EVs based on flight schedule and sequencing algorithm, as shown in Figure. 3. The SOC of each electric vehicle in the airport is initialized with a random uniform distribution.

Each EV in the airport has many variables in the "vehicle matrix", and each EV includes the state of charge (SOC), availability, current state, and tag number [30]. Availability  $\lambda_{EV}$ , which is affected by SOC and current state, denotes the available number of EVs with SOC greater than SOC<sub>min</sub> at each time slot. The current state is used to indicate whether the electric vehicle is charging. The number of planes coming in at the given time slot determines how many EVs are required.  $D_{\rm EV}(t)$  denotes the EVs in working state at each time slot, which is equal to the number of aircraft multiplied by EV required for each aircraft. For every time slot, each EV is ranked and recorded according to the attributions within the vehicle matrix. EVs with lower SOC will have higher ranks and thus have charging priority over other EVs. EVs with higher SOC will have dispatch priority to serve aircraft. If the number of uncharged EVs(  $N_{uchg}(t)$  ) meets the service demand at period t, EVs that are currently charged will not serve aircraft, even if its current SOC is high.

When the EVs' availability is insufficient at a time step to cover the required aircraft ground service, gas vehicles are used to fill the shortage. The number of EVs that can be charged at any time is mainly determined by the number of charging piles ( $N_{CP}$ ) and EVs that have not been dispatched ( $N_{udp}(t)$ ). At each time slot t, the SOC of each EV will be updated. If the EV is charging, the SOC increases by the charging rate during the time step (Equation (9)). Conversely, the SOC decreases by the energy consumption rate if it services an aircraft at the time step (Equation (10)) The EV dispatch algorithm aims to maximize the numbers of EV usage for the whole period of 24 hours.

$$SOC_t^{final} = SOC_t^{initial} + SOC_t^{charge}$$
 (9)

$$SOC_{t}^{final} = SOC_{t}^{initial} - SOC_{t}^{service}$$
 (10)

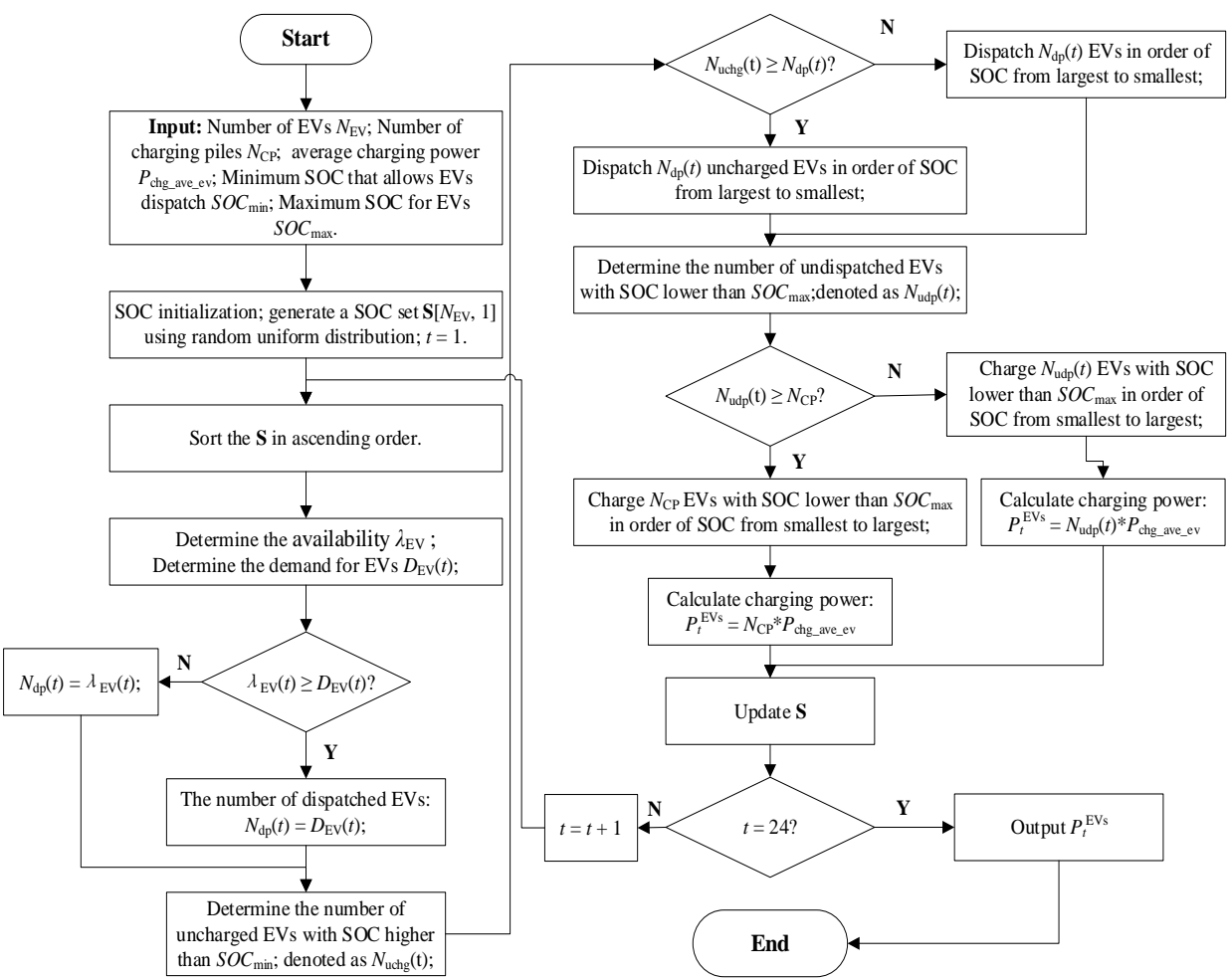


Fig. 3. Flow chart of EVs charging load profile

### B. Optimization of the HIES

The objective function is expressed in Equations (11)-(14) to minimize the overall economic cost of HIES by considering the capital cost, operating cost, and carbon emission cost. The objective function is formulated as follows:

$$Min \ \varphi = \frac{j(1+j)^{N}}{(1+j)^{N}-1} \sum_{y=0}^{N} \frac{C_{y}^{inv}}{(1+j)^{y}} + C^{op} + C^{emission}$$
(11)
$$C_{y}^{inv} = \sum_{i \in device} \{ \psi_{i}^{cap}(y=0) + \pi_{i}^{rep} \psi_{i}^{cap}(\text{device } i \text{ is } \text{replaced } at \text{ year } y) - \pi_{i}^{rep} \psi_{i}^{cap} \frac{l_{i}^{rem}}{l_{i}^{comp}}(y=N) \}$$
(12)
$$C^{op} = \sum_{t=1}^{T} \pi_{t}^{electricity \ price} P_{t}^{grid, huy} \Delta t + \sum_{m=1}^{12} \pi^{demand} P_{month}^{demand, max} +$$
(13)
$$\sum_{i \in \Omega^{device}} \pi_{i}^{m} \psi_{i}^{cap} + \sum_{t=1}^{T} \pi^{shortage, H_{2}} m_{t}^{shortage, H_{2}} - \sum_{t=1}^{T} \pi^{Oxygen \ price} m_{t}^{out, O_{2}} \Delta t$$

$$C^{emission} = \pi^{emission} \sum_{t=1}^{T} d_{grid}^{emission} P_{t}^{grid, buy} \Delta t$$
(14)

where  $C_y^{inv}$  denotes the investment cost within y years, which includes the initial investment in year 0, the replacement cost of equipment during the project cycle and the salvage value of equipment at the end of the project

cycle, Cop represents the annual operating cost, which includes the purchase cost of electricity, equipment operation and maintenance cost, penalty cost of unmet hydrogen, and revenue from the sale of oxygen, C<sup>emission</sup> denotes the annual carbon emission cost derived from power grid; j denotes the discount rate, N denotes the project lifecycle,  $\pi_i^{inv}$  represents the unit investment cost of device i,  $\psi_i^{cap}$  denotes the capacity of device i (kW, kWh),  $\pi_i^{rep}$  denotes the unit replacement cost of equipment i,  $l_i^{comp}$  represents the lifetime of device i,  $l_i^{rem}$  represents the residual lifetime of device i, T denotes the number of time slots,  $\pi_t^{electricity \ price}$  denotes the electricity price at time slot t (Y/kWh),  $\pi^{demand}$  denotes the cost of power demand( Y/kW),  $\pi_i^m$  denotes the unit maintenance cost of device i (Y/kW),  $\pi^{shortage,H_2}$  denotes the penalty cost of hydrogen shortage (Y/kg),  $m_t^{shortage,H_2}$  is the hydrogen shortage at time slot t,  $\pi^{Oxygen\ price}$  denotes the price of oxygen,  $\pi^{emission}$ represents the unit carbon tax(Y/kg), and  $d_{grid}^{emission}$  denotes the unit carbon emission(kg/kWh).

The proposed airport energy systems model is subject to both planning and operation constraints. All constraints were applied to each time interval within the optimization time horizon. Equation (15) provides the constraint of electricity supply and demand balance, while Equation (16) expresses the constraint of hydrogen capacity required by fuel cell. Equation

(17) expresses the constraint of device capacity, Equation (18) expresses the power constraint of PV, electrolyzer, and fuel cell, Equation (19) expresses the BSS constraint, and Equation (20) expresses the constraint of the hydrogen storage tank.

$$P_{t}^{grid,buy} + P_{t}^{pv} + P_{t}^{out,BSS} - P_{t}^{in,BSS} = P_{t,contact \ stands}^{aircrafts} + P_{t}^{EVs} + P_{t}^{in,electrolyzer}$$

$$P_{t}^{FC} = P_{t,contact \ stands}^{aircraft} + P_{t}^{EVs} + P_{t}^{in,electrolyzer}$$

$$F_{t}^{FC} - m_{t}^{shortage,H_{2}} = m_{t}^{out,H_{2}} + m_{t,H_{2}}^{s,out} - m_{t,H_{2}}^{s,in}$$

$$\sum_{t=0}^{T} m_{t}^{shortage,H_{2}} \leq \lambda^{shortage,H_{2}} \sum_{t=0}^{T} F_{t}^{H_{2}}$$
(15)

$$\sum_{t=1}^{T} m_t^{shortage, H_2} \le \lambda^{shortage, H_2} \sum_{t=1}^{T} F_t^{H_2}$$

$$0 \le m_t^{shortage, H_2} \le F_t^{H_2}$$
(16)

$$0 \le m_t^{shortage, H_2} \le F_t^{H_2}$$

$$\psi_i^{cap,\min} \le \psi_i^{cap} \le \psi_i^{cap,\max} \tag{17}$$

$$\begin{cases} 0 \leq P_{t}^{pv} \leq P_{t,pv}^{out} \\ P_{\min}^{in,electrolyzer} \leq P_{t}^{in,electrolyzer} \leq P_{\max}^{in,electrolyzer} \\ P_{\min}^{FC} \leq P_{t}^{FC} \leq P_{\max}^{FC} \end{cases}$$
(18)

$$\begin{cases} 0 \le P_t^{in,BSS} \le u(t) P_{\text{max}}^{in,BSS} \\ 0 \le P_t^{out,BSS} \le (1 - u(t)) P_{\text{max}}^{out,BSS} \\ E^{\min} \le E_t^{BSS} \le E^{\max} \end{cases}$$
 (19)

$$\begin{cases} v(t)m_{\min,H_{2}}^{s,in} \leq m_{t,H_{2}}^{s,in} \leq v(t)m_{\max,H_{2}}^{s,in} \\ (1-v(t))m_{\min,H_{2}}^{s,out} \leq m_{t,H_{2}}^{s,out} \leq (1-v(t))m_{\max,H_{2}}^{s,out} \\ m_{\min,H_{2}}^{s} \leq m_{\max,H_{2}}^{s} \end{cases}$$
 (20)

where  $\psi_i^{cap, \min}$  and  $\psi_i^{cap, \max}$  represent the upper and lower limits of device capacity,  $p_{\min}^{in, electrolyzer}$  and  $P_{\max}^{in, electrolyzer}$  represent the upper and lower limits of electrolyzer power,  $P_{\min}^{FC}$  and  $P_{\text{max}}^{FC}$  represent the upper and lower limits of fuel cell generation,  $P_{\text{max}}^{in,BSS}$  and  $P_{\text{max}}^{out,BSS}$  represent the maximum charging/discharging power of BSS, u(t) denotes the constraint parameter of BSS,  $E^{min}$  and  $E^{max}$  represent the upper and lower limits of BSS capacity,  $m_{\min,H_2}^{s,in}$  and  $m_{\max,H_2}^{s,in}$ represent the upper and lower limits of  $m_{t,H_2}^{s,in}$ ,  $m_{\min,H_2}^{s,out}$  and  $m_{\max,H_2}^{s,\text{out}}$  represent the upper and lower limits of  $m_{t,H_2}^{s,\text{out}}$ ,  $m_{t+1,H_2}^{s}$ and  $m_{t,H_2}^s$  represent the stored hydrogen capacity at time slots t+1 and t,  $m_{\min,H_2}^s$  and  $m_{\max,H_2}^s$  represent the upper and lower limits of stored hydrogen, u(t) and v(t) denote the constraint parameter for BSS and Hydrogen storage tank.

#### C. Resilience assessment model

The major difference between the resilience assessment for the airport energy system and the general resilience assessment is that the setting of parameters affects the resilience assessment results, in addition to considering the performance changes of the system. The damage and recovery degree of the system will be different in different disaster times. Therefore, the resilience index of the airport energy system is divided into two dimensions: the temporal performance index and the system's overall performance index. The resilience assessment for airport energy systems must necessarily be associated with disaster time. However, the disaster time is related to airport energy demand, which can be a fixed time or change with the situation. In the process of airport operation, it is impossible to fully predict the time and

scale of disaster, and the disaster has strong randomness. In order to meet the operation of airport energy system, the system can only operate normally when the system has the performance above the minimum threshold.

In summary, a resilience assessment for airport energy systems should not only consider the changes of system performance, but also consider the disaster time, the minimum performance requirements and the randomness of disturbance. Therefore, it is urgent to establish a resilience assessment method for airport energy system, which should combine the disaster time and demand, so as to reflect the resilience of airport energy system to the randomness of disturbance.

When the electricity supply of airport energy system is insufficient, the performance will fluctuate. The performance curve of airport energy system at time slots  $T_0$  and T, is shown in Figure. 4.

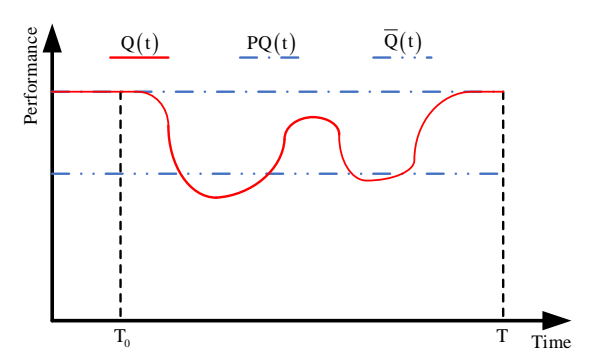


Fig. 4. System performance curve

Q(t) is the unit performance of the airport energy system at time t, which is expressed as the ratio of the total output of the grid, PV, BSS, and hydrogen energy system to the electrical load of the airport,  $0 \le Q(t) \le 1$ . PQ(t) is the best performance of airport energy system at time t.  $\gamma(t) \in [0,1]$ is the performance requirement parameter, Q(t) is the minimum performance requirements of the airport energy system at time t, as shown in (21).

$$\overline{Q}(t) = \gamma(t) * Q(t) \tag{21}$$

The resilience assessment index for the airport energy system is as follows:

$$R_{\alpha}\left(T\right) = \frac{\int_{T_{0}}^{T} Q(t)^{\alpha} \left[Q(t) - \overline{Q}(t) \ge 0\right] dt}{\int_{T_{0}}^{T} PQ(t)^{\alpha} dt}$$
(22)

where  $|Q(t)-\overline{Q}(t)| \ge 0$  is the inversion bracket, if and only if  $Q(t) - \overline{Q}(t) \ge 0$  is true,  $|Q(t) - \overline{Q}(t) \ge 0| = 1$ , otherwise  $Q(t) - \overline{Q}(t) \ge 0$  = 0.  $\alpha \in \{0,1\}$  is the handover parameter between temporal performance and system overall performance.

When  $\alpha = 0$ ,  $R_0(T)$  is the temporal performance index of system, and this parameter describes the ratio of the total time for the airport energy system to meet minimum performance requirements at time  $T \square T_0$ .  $R_0(T)$  describes the problem of whether the performance is degraded below the minimum performance requirement for the airport energy system after the energy supply is insufficient on the main grid side, and the

speed of the electricity supply from failing to meet the electricity supply requirements to restore the minimum performance requirements. A larger value represents that the airport energy system can quickly recover to above the minimum performance requirements after suffering the energy supply shortage.  $\max(R_0(T)) = 1$  shows that the performance of the airport energy system is higher than Q(t)in the current period, and the current impact is not enough to hinder the normal operation of the airport.  $\min(R_0(T)) = 0$ shows that the energy supply of the airport energy system is unable to meet the minimum requirements in the current period, and the current impact of the airport energy system has been unable to meet the minimum energy requirements. In addition,  $R_0(T)$  is a function of time T, which reflects the accumulation of all impacts of the airport energy system at different times.

When  $\alpha=1$ ,  $R_1(T)$  is the system overall performance index of system, which describes the closeness between the actual performance and the best (expectations) performance PQ(t) of airport energy system in the effective period, and the ratio of the actual effective performance accumulation to the best performance accumulation of airport energy system in the operation time. Presumably, the actual performance of airport energy system does not exceed the best performance,  $Q(t) \leq PQ(t)$ , from (22):

$$0 \le R_1(T) \le \frac{\int_{T_0}^T PQ(t) \left[ Q(t) - \overline{Q}(t) \ge 0 \right] dt}{\int_{T_0}^T PQ(t) dt} = R_0(T) \quad (23)$$

Therefore  $0 \le R_1(T) \le R_0(T) \le 1$ .  $R_0(T)$  is the best situation of  $R_1(T)$ , and the airport energy system is restored to the minimum performance requirements at the same time to achieve the best performance.

Based on the above derivation,  $R_0(T)$  considers the cumulative time situation of the airport energy system to meet the minimum performance requirements, but not the degree of performance for the airport energy system above the power supply-demand capacity.  $R_1(T)$  focuses on the degree of performance recovery but lacks the reflection of whether the airport energy system meets the recovery time. Therefore, to get a better understanding of the overall performance of an airport energy system, a comprehensive resilience index is proposed based on two dimensions of temporal performance and system overall performance as follows:

$$R(T) = \beta R_0(T) + (1 - \beta) R_1(T) \tag{24}$$

where  $\beta$  is the resilience focus factor of the airport energy system,  $0 \le \beta \le 1$ , with  $0 \le R(T) \le 1$ . When the ability of airport energy system needs to be focused on maintaining the minimum demand performance after the power supply is insufficient on the main grid side, a larger  $\beta$  can be set to make the comprehensive resilience index focus on the temporal performance of airport energy system. When the research on the degree of performance recovery and accumulation of airport energy system needs to be focused on during the  $T_0 \square T$  time period after the power supply is insufficient on the main grid side, a smaller  $\beta$  can be set to make the comprehensive resilience index focus on the system

overall performance of airport energy system.

The characteristics of the proposed comprehensive resilience assessment index can therefore be summarized as:

- 1) The comprehensive resilience assessment index of the airport energy system proposed is a function with time *T* as the independent variable. Even if the airport energy system is faced with the same disturbance, it will show different resilience values at different times. Therefore, this index can not only predict the trend of the system with the change of resilience over time but also evaluate the resilience throughout the whole time.
- 2) The resilience assessment method fully utilizes the system performance curve Q(t) and does not divide the intermediate process of resilience into stages. Therefore, it is not affected by the random characteristics of disturbance and recovery process, and the evaluation of airport energy system is effective with a comprehensive resilience index.
- 3) The index reflects the resilience of the system from two dimensions of time and performance and evaluates the system resilience by combining the resilience focus factor and actual demand, focusing on time or performance.
- 4) According to the method proposed in this section, the resilience of the system can be improved by changing the permeability of hydrogen energy, which is simple and efficient.

### IV. CASE STUDY

### A. Case Description

The part of the flight schedule of an airport on a typical day is shown in Table.1, an hourly-based aircraft APU load characteristic model is established to obtain a new electric load profile of aircraft. The arrival/departure flow curves from different terminals on a typical day are obtained based on flight schedule as shown in Figure. 5. Figure. 6 shows the electric load profile of aircraft on a typical day. Figure. 7 shows the EV charging load profile on a typical day. The charging load is very low during 05:00-09:00 due to the fewer flight schedules within this period but the EVs are already in full charge state before 05:00, and the initial flight peak period is during 06:00-09:00.

Based on the model of the airport energy system, the power supply capacity of the main grid side is reduced to 80%, 70%, and 60% of the benchmark value, which simulates the insufficient power supply of airport energy system when the main grid side encounters natural disasters or abrupt failures. Furthermore, the proportion of hydrogen energy in the airport energy system is changed to make the permeability varying at 20%, 30%, and 40%. The resilience assessment of HIES was conducted under the combinations of these different energy supply scenarios.

The parameters of the airport example used in the paper are set as follows:

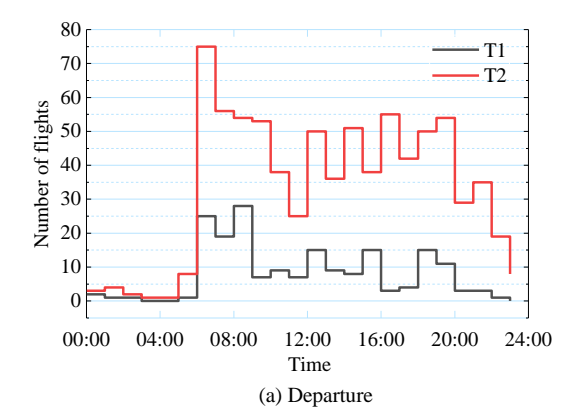
1) The maximum PV generation capacity of 40 MW is an indicative figure, which can vary according to the different airport sizes with land space. The average

- ambient temperature and annual global radiations are 13.33°C and 3.59 kWh/m²/day, respectively.
- 2) The bus voltage of the energy storage system is designed to be 600 V, consisting of 100 1kWh/6V lithium batteries connected in series.
- 3) The directly connected electric demand in the airport energy system is aircraft (APU replacement) at contact stands and EVs. The indirect electric demand is the aircraft (APU replacement) at remote stands.
- 4) The annual electric demand of the airport energy system is calculated according to the flight schedule and other external factors. Figure. 8 shows the annual electric demand profile of HIES.
- 5) The economic cost of the airport energy system includes capital investment, maintenance of various energy devices as summarized in Table.2. The electricity price on the main grid side and oxygen price as summarized in Table.3.

TABLE 1. PART OF THE FLIGHT SCHEDULE OF AN AIRPORT ON A TYPICAL DAY

|            | (a)Flight departure time and terminal |                     |                   |          |          |  |  |  |  |
|------------|---------------------------------------|---------------------|-------------------|----------|----------|--|--|--|--|
| Flight No. | From                                  | То                  | Departure<br>Time | Terminal | Take Off |  |  |  |  |
| YG9028     | CHENGDU                               | XI'AN               | 04:20             | T2       | 04:29    |  |  |  |  |
| 3U3713     | CHENGDU                               | BRUXELLES           | 04:35             | T1       | 06:33    |  |  |  |  |
| CX2061     | CHENGDU                               | HONGKONG            | 04:45             | T2       | 05:12    |  |  |  |  |
| CA403      | CHENGDU                               | SINGAPORE<br>CHANGL | 05:00             | T2       | 05:18    |  |  |  |  |
| UA2802     | CHENGDU                               | TOKYO NARITA        | 05:15             | T2       | 05:07    |  |  |  |  |
| 3U8225     | CHENGDU                               | BRUXELLES           | 05:40             | T1       | 06:00    |  |  |  |  |
| Y87938     | CHENGDU                               | SHANGHAI<br>PUDONG  | 05:50             | T2       | 06:19    |  |  |  |  |

|            | (b) Fli          | ght arrival time | and terminal      |          |        |  |
|------------|------------------|------------------|-------------------|----------|--------|--|
| Flight No. | From             | То               | Departure<br>Time | Terminal | Arrive |  |
| MU2230     | HEFEI            | CHENGDU          | 00:25             | T2       | 23:19  |  |
| 3U8814     | DALIAN           | CHENGDU          | 00:20             | T1       | 23:55  |  |
| MU4050     | DALIAN           | CHENGDU          | 00:20             | T1       | 23:55  |  |
| 3U8570     | DUNHUANG         | CHENGDU          | 00:20             | T1       | 23:46  |  |
| EU2240     | FUZHOU           | CHENGDU          | 00:25             | T2       | 23:50  |  |
| HO3475     | FUZHOU           | CHENGDU          | 00:25             | T2       | 23:50  |  |
| CA1238     | <b>ZHANIIANG</b> | CHENGDII         | 00.25             | T2       | 00:01  |  |



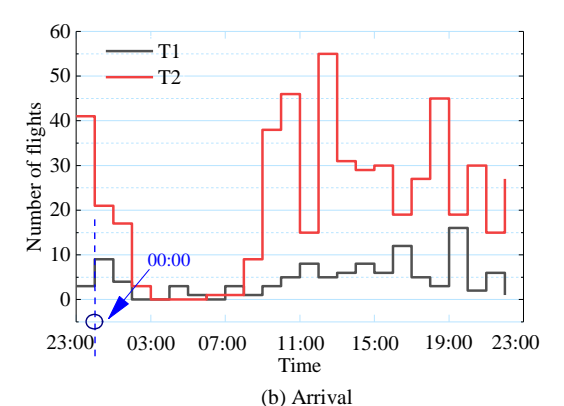


Fig. 5. Number of flight arrival/departure on a typical day

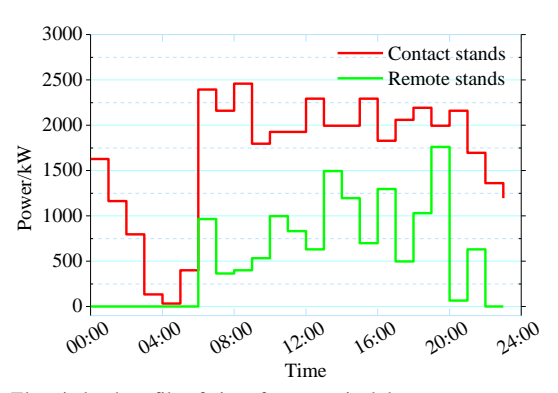


Fig. 6. Electric load profile of aircraft on a typical day

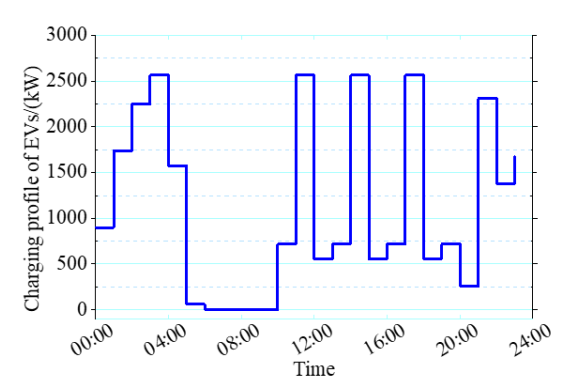
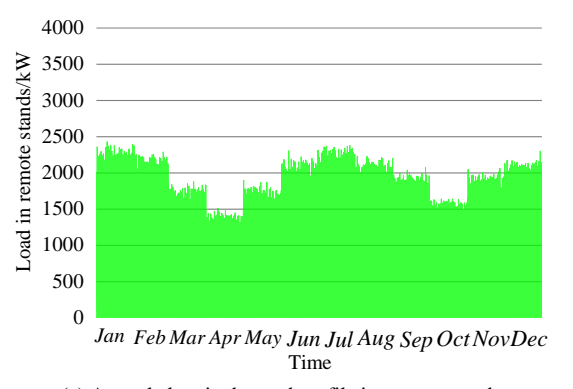
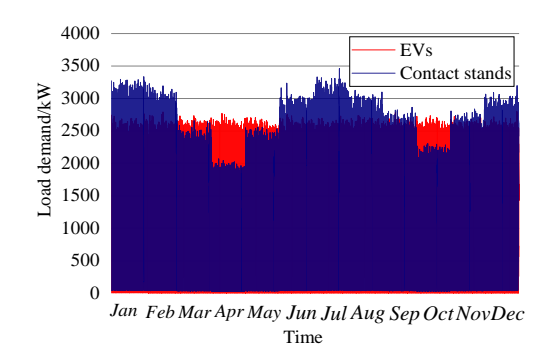


Fig. 7. Charging load profile of EVs in airport



(a) Annual electric demand profile in remote stands



(b) Annual electric demand of EVs and aircraft in contact stands Fig. 8. Annual electric demand profile of HIES

 ${\bf TABLE~2.}$  THE ENERGY DEVICES ECONOMIC COSTS OF HIES FOR AIRPORT

| Energy device | Capital   | Maintenance | Replacemen | t<br>Life time(years) |
|---------------|-----------|-------------|------------|-----------------------|
| Electrolyzer  | 4246¥/kW  | 442.9 ¥/kW  | -          | 25                    |
| Hydrogen tank | 9000¥/kW  | 105¥/kg     | -          | 25                    |
| Fuel cell     | 3366¥/kW  | 77.605¥/kW  | 2925 ¥ /kW | 5                     |
| PV            | 3851 ¥/kW | 56.56 ¥/kW  | -          | 25                    |
| BSS           | 700¥/kW   | 35¥/kW      | 627¥/kW    | 10                    |
| Grid          | -         | -           | -          | -                     |

As shown in Table 2, the BSS is replaced twice during the entire lifecycle in the 10th and 20th years, respectively, and the fuel cell of the hydrogen energy system is replaced four

times during the entire lifecycle in the 5th, 10th, 15th, and 20th years, respectively.

TABLE 3.
THE ELECTRIC PRICE AND OXYGEN PRICE

|                   | Time interval            | price                                  |
|-------------------|--------------------------|--|
|                   | 23:00-6:00               | 0.56 ¥/kWh                             |
| Electricity price | 7:00-9:00; 14:00-17:00   | 0.87 ¥/kWh                             |
|                   | 10:00-13:00; 18:00-22:00 | 1.3  Y/kWh                             |
| Oxygen price      | -                        | 35 ¥/bottle (15MPa,<br>40L)/ 4.08 ¥/kg |

# B. Analysis of Case Results

This paper analyzes the resilience of different energy configuration schemes for HIES using realistic airport data. The testing scenarios are created by combining the different reductions to the power capacity of the main grid and the different hydrogen penetration levels.

Scenario  $A_{0.8}^{0.2}$  was used to represent the operation scenario, in which the electric supply capacity of the main grid side was reduced to 80% of the reference value in the airport energy system with hydrogen permeability of 20%. The optimization results of HIES and the evaluation results of comprehensive resilience indices in scenario  $A_{0.8}^{0.2}$ ,  $A_{0.8}^{0.3}$ ,  $A_{0.8}^{0.4}$ ,  $A_{0.7}^{0.2}$ ,  $A_{0.7}^{0.3}$ ,  $A_{0.6}^{0.4}$ ,  $A_{0.6}^{0.2}$ ,  $A_{0.6}^{0.3}$ , and  $A_{0.6}^{0.4}$ , are shown in Table.4 and Table 5.

TABLE 4. OPTIMIZATION RESULTS IN DIFFERENT SCENARIOS

| Scenarios                     | Electrolyzer (MW) | Hydrogen tank(kg) | Fuel<br>cell<br>(MW) | PV(MW) | BSS(MW) | Total annual cost ( Y million) |
|-------------------------------|-------------------|-------------------|----------------------|--------|---------|--------------------------------|
| A <sub>1</sub> <sup>0.2</sup> | 7.5               | 1550              | 2.45                 | 33.951 | 17.8    | 3.725                          |
| $A_1^{0.3}$                   | 11.8              | 2439              | 3.85                 | 32.987 | 21.1    | 5.861                          |
| $A_1^{0.4}$                   | 16.5              | 3410              | 5.39                 | 33.426 | 24.4    | 8.195                          |
| $A_{0.8}^{0.2}$               | 8.1               | 1674              | 2.65                 | 36.67  | 19.4    | 4.023                          |
| $A_{0.8}^{0.3}$               | 12.5              | 2583              | 4.08                 | 57.877 | 30.1    | 6.208                          |
| $A_{0.8}^{0.4}$               | 17.2              | 3551              | 5.61                 | 77.984 | 40.6    | 8.543                          |
| $A_{0.7}^{0.2}$               | 8.6               | 1775              | 2.81                 | 39.212 | 21.3    | 4.271                          |
| $A_{0.7}^{0.3}$               | 13.0              | 2684              | 4.25                 | 59.465 | 31.9    | 6.456                          |
| $A_{0.7}^{0.4}$               | 17.6              | 3629              | 5.75                 | 80.546 | 41.5    | 8.74                           |
| $A_{0.6}^{0.2}$               | 9.0               | 1840              | 2.94                 | 41.012 | 21.2    | 4.469                          |
| $A_{0.6}^{0.3}$               | 13.4              | 2769              | 4.38                 | 62.012 | 31.6    | 6.654                          |
| $A_{0.6}^{0.4}$               | 17.9              | 3685              | 5.85                 | 83.014 | 42.1    | 8.887                          |

# TABLE 5. EVALUATION RESULTS OF RESILIENCE INDEXES (a) The power supply capacity of the main grid side is reduced to 80%.

| Scenarios           | Minimum performance – | Comprehensive resilience $R(T)$ |               |       |  |
|---------------------|-----------------------|---------------------------------|---------------|-------|--|
| Scenarios           | ratio                 | β=0                             | $\beta = 0.5$ | β=1   |  |
| ${f A}_{0.8}^{0.2}$ | 60%                   | 0.731                           | 0.705         | 0.686 |  |
|                     | 70%                   | 0.623                           | 0.618         | 0.611 |  |
|                     | 80%                   | 0.536                           | 0.505         | 0.498 |  |
|                     | 60%                   | 0.801                           | 0.789         | 0.769 |  |
| $A_{0.8}^{0.3}$     | 70%                   | 0.694                           | 0.684         | 0.672 |  |
|                     | 80%                   | 0.603                           | 0.572         | 0.567 |  |
|                     | 60%                   | 0.859                           | 0.831         | 0.812 |  |
| $A_{0.8}^{0.4}$     | 70%                   | 0.752                           | 0.741         | 0.729 |  |

(b) The power supply capacity of main grid side WAS reduced to 70%.

0.665

0.638

0.614

80%

| Scenarios       | Minimum performance – | Comprehensive resilience $R(T)$ |               |           |  |
|-----------------|-----------------------|---------------------------------|---------------|-----------|--|
| Scenarios       | ratio                 | $\beta=0$                       | $\beta = 0.5$ | $\beta=1$ |  |
|                 | 60%                   | 0.681                           | 0.687         | 0.632     |  |
| $A_{0.7}^{0.2}$ | 70%                   | 0.584                           | 0.569         | 0.564     |  |
|                 | 80%                   | 0.492                           | 0.471         | 0.441     |  |
|                 | 60%                   | 0.751                           | 0.740         | 0.726     |  |
| $A_{0.7}^{0.3}$ | 70%                   | 0.662                           | 0.644         | 0.648     |  |
|                 | 80%                   | 0.570                           | 0.552         | 0.519     |  |
| $A_{0.7}^{0.4}$ | 60%                   | 0.812                           | 0.795         | 0.758     |  |
| $\Lambda_{0.7}$ | 70%                   | 0.709                           | 0.691         | 0.681     |  |

| 80% | 0.629 | 0.696 | 0.573 |
|-----|-------|-------|-------|
|     |       |       |       |

(c) The power supply capacity of main grid side was reduced to 60%.

| Scenarios       | Minimum performance – | Comprehensive resilience $R(T)$ |               |       |
|-----------------|-----------------------|---------------------------------|---------------|-------|
| Scenarios       | ratio                 | β=0                             | $\beta = 0.5$ | β=1   |
|                 | 60%                   | 0.624                           | 0.624         | 0.576 |
| $A_{0.6}^{0.2}$ | 70%                   | 0.531                           | 0.506         | 0.495 |
|                 | 80%                   | 0.439                           | 0.403         | 0.397 |
|                 | 60%                   | 0.699                           | 0.685         | 0.668 |
| $A_{0.6}^{0.3}$ | 70%                   | 0.605                           | 0.585         | 0.579 |
|                 | 80%                   | 0.513                           | 0.498         | 0.468 |
|                 | 60%                   | 0.764                           | 0.732         | 0.692 |
| $A_{0.6}^{0.4}$ | 70%                   | 0.653                           | 0.636         | 0.623 |
|                 | 80%                   | 0.578                           | 0.634         | 0.516 |

Table 4 illustrates the optimal sizing results of energy devices at different airport energy system scenarios. By reducing the main grid side power supply capacity of the airport energy system, the electrolyzer capacity, hydrogen tanks capacity, fuel cell capacity, PV capacity, BSS capacity, and the total annual cost will be increased. When the main grid side power supply capacity of the airport energy system was reduced from 80% to 60%, the capacity of the hydrogen energy system increased by nearly 12%, the PV energy capacity increased by nearly 11%, the capacity of the battery storage system increased by nearly 10%, and the total annual cost increased by nearly 11%. This finding shows that when the energy demand of the airport is insufficient, the airport energy system can meet the load demand of the airport by increasing the capacity of different energy forms in the airport. However, the total annual cost for HIES will be increased.

The disaster time T is set to 6h, and the effects of  $\beta$  and  $\overline{Q}(t)$  on the result of the comprehensive resilience assessment were studied. The two major factors that affect the proposed comprehensive resilience index are  $\beta$  value and the minimum performance ratio. When  $\beta$  was set to a constant, the comprehensive resilience index decreased with the increase in minimum performance ratio of the airport energy system, and the comprehensive resilience index increased with the increase in the hydrogen penetration of airport energy system; When the minimum performance ratio was set to constant, the comprehensive resilience index decreased with the increase in  $\beta$  value. As the main grid side power supply capacity of the airport energy system decreased, the comprehensive resilience index also decreased.

As shown in Table.5, when  $\beta=0$ , comprehensive resilience R(T) is referred to as the system's overall performance  $R_1(T)$ , and  $R_1(T)$  focuses on the degree of performance recovery and lacks the reflection of whether the airport energy system meets the recovery time. When  $\beta=1$ , the comprehensive resilience R(T) is referred to as the temporal performance  $R_0(T)$ , while  $R_0(T)$  considers the cumulative time situation of the airport energy system to meet the minimum performance requirements, and does not consider the degree of performance for the airport energy system above the power supply-demand capacity.

Also in Table 5, when the energy supply of the airport energy system is affected, the resilience of the airport energy system can be improved by increasing the hydrogen energy permeability of the airport energy system. When the hydrogen permeability of the airport energy system was increased from 20% to 40%, the comprehensive resilience index of the airport energy system was improved by nearly 18%. At this time, the resilience of the airport energy system has increased significantly.

TABLE 6.
EVALUATION RESULTS UNDER DIFFERENT DISASTER TIMES
(a) The power supply capacity of the main grid side was reduced to 80%

| (a) The power supply capacity of the main grid side was reduced to 80%. |            |              |             |            |           |        |
|---|------------|--------------|-------------|------------|-----------|--------|
| C :   | β          |              | dis         | aster time | /h        |        |
| Scenarios   | $\rho$     | 2            | 4           | 6          | 8         | 10     |
|   | 0          | 0.511        | 0.57        | 0.623      | 0.678     | 0.737  |
|   | 0.25       | 0.506        | 0.565       | 0.62       | 0.675     | 0.732  |
| $A_{0.8}^{0.2}$   | 0.5        | 0.498        | 0.554       | 0.618      | 0.674     | 0.731  |
|   | 0.75       | 0.492        | 0.551       | 0.614      | 0.669     | 0.728  |
|   | 1          | 0.487        | 0.546       | 0.611      | 0.664     | 0.719  |
| (b) The po  | wer supply | y capacity o | f main grid | l side was | reduced t | o 70%. |
| Scenarios   | β          |              | dis         | aster time | /h        |        |
| Scenarios   | P          | 2            | 4           | 6          | 8         | 10     |
|   | 0          | 0.476        | 0.528       | 0.584      | 0.638     | 0.698  |
|   | 0.25       | 0.473        | 0.522       | 0.577      | 0.636     | 0.696  |
| $A_{0.7}^{0.2}$   | 0.5        | 0.468        | 0.517       | 0.569      | 0.631     | 0.692  |
|   | 0.75       | 0.462        | 0.511       | 0.566      | 0.627     | 0.688  |
|   | 1          | 0.455        | 0.507       | 0.564      | 0.624     | 0.679  |
| (c) The po  | wer supply | y capacity o | f main grid | side was   | reduced t | o 60%. |
| Cooponios   | В          |              | dis         | aster time | /h        |        |
| Scenarios   | β          |              | -           |            | 0         | 10     |

| Scenarios           | β    | disaster time/h |       |       |       |       |
|---------------------|------|-----------------|-------|-------|-------|-------|
|                     |      | 2               | 4     | 6     | 8     | 10    |
| ${f A}_{0.6}^{0.2}$ | 0    | 0.428           | 0.479 | 0.531 | 0.585 | 0.644 |
|                     | 0.25 | 0.421           | 0.475 | 0.519 | 0.582 | 0.642 |
|                     | 0.5  | 0.416           | 0.468 | 0.506 | 0.576 | 0.635 |
|                     | 0.75 | 0.411           | 0.461 | 0.501 | 0.567 | 0.627 |
|                     | 1    | 0.399           | 0.452 | 0.495 | 0.556 | 0.604 |

As shown in Table.6, the resilience of the airport energy system was calculated respectively when the disaster time T was 2h, 4h, 6h, 8h and 10h. The hydrogen permeability of the airport energy system is set at 30%, PQ(t) = 100%, Q(t) = 70%. when  $\beta = 0$ ,  $R_0(T)$  is the optimal situation of system resilience. In this case, any system whose performance is higher than the minimum requirement is considered to meet the system requirements. However,  $R_1(T)$  further considers the degree of recovery when meeting the minimum requirements. The closer the level of recovery is to Q(t), the closer  $R_1(T)$  is to  $R_0(T)$ . With the increase of  $\beta$ , the comprehensive resilience index changes from system overall performance to temporal performance. As the main grid side power supply capacity of the airport energy system decreased, the comprehensive resilience index also decreased.

# V. CONCLUSION

The electrification of the airport energy system is an inevitable development trend in the future to mitigate carbon emissions. The deployment of hydrogen resources is a promising solution to increase renewable power generation, therefore an energy system with high penetration of hydrogen resources for the airport is proposed. Based on passenger' travel behavior, an aircraft load characteristic model is developed to quantify the electrified aircraft load which replaces the fuel-powered APU. A vehicle matrix method for generating EVs charging profile based on flight schedule and

sequencing algorithm is proposed to make full use of EV in the airport. A MILP optimization method is developed to design the optimal capacity of each energy device of the airport microgrid. A comprehensive resilience index and enhancement strategy are proposed for HIES. The grid side power supply capacity of the airport energy system was reduced, and this scenario simulates the insufficient power supply of the airport energy system to explore the resilience of the airport energy system when the grid encounters natural disasters or abrupt failures. The key findings are summarized as follows:

- The hydrogen integrated energy system proposes an economic and environmentally friendly solution to design the future airport energy system. when the energy demand of the airport is insufficient, the airport energy system can meet the load demand of the airport by increasing the capacity of different energy forms in the airport. However, the total annual cost for HIES will be increased.
- When the main grid side power supply capacity of the airport energy system is reduced from 80% to 60%, the capacity of the hydrogen energy system increased by nearly 12%, the PV energy capacity increased by nearly 11%, and the capacity of BSS increased by nearly 10%.
- 3) When the hydrogen permeability of the airport energy system was increased from 20% to 40%, the comprehensive resilience index of the airport energy system was improved by nearly 18%, and the resilience of the airport energy system has increased significantly at this time. With the increase of the disaster time, the comprehensive resilience index decreased.

This article puts resilience research in the airport microgrid system, which has certain limitations. The next step of the research will be established in a general scenario, and the power flow constraint will also be included in the overall framework. We consider these as valuable future work to address the limitations not only on technical aspects but also on policy and other factors.

#### REFERENCES

- IEA, "CO2 emissions statistics 2018 accessed 15 January 2019," 2018. https://www.iea.org/statistics/co2emissions/.
- [2] B. J. Brelje and J. Martins, "Electric, hybrid, and turboelectric fixed-wing aircraft: A review of concepts, models, and design approaches," *Prog. Aerosp. Sci.*, vol. 104, pp. 1-19, 2019.
- [3] J. Zhang et al., "Integrated photovoltaic and battery energy storage (PV-BES) systems: An analysis of existing financial incentive policies in the US," Appl. Energy, vol. 212, pp. 895-908, 2018.
- [4] F. Dawood, M. Anda, and G. M. Shafiullah, "Hydrogen production for energy: An overview," *Int. J. Hydrogen Energy*, vol. 45, no. 7, pp. 3847-3869, 2020.
- [5] E. L. V. Eriksson and E. M. Gray, "Optimization and integration of hybrid renewable energy hydrogen fuel cell energy systems - A critical review," *Appl. Energy*, vol. 202, pp. 348-364, 2017.
- [6] President's Council of Economic Advisers and the U.S. Department of Energy's Office of Electricity and Energy Reliability, "Economic benefits of increasing electric grid resilience to weather outages," Executive Office of the President, U.S. Dept. Energy, Washington, DC, USA, Tech. Rep., Aug. 2013. [Online]. Available: http://energy.gov/ sites/prod/files/2013/08/f2/Grid%20Resiliency%20Report\_FINAL.pdf
- [7] Z. Bie et al., "Development and prospect of resilient power system in the context of energy transition," *Proc. CSEE*, vol. 40, no. 9, pp. 2735-2745, 2020.
- [8] P. Sun et al., "Research status and development of DC distribution network," *Electric Power Autom. Equip.*, vol. 36, no. 6, pp. 64-73, 2016.

- [9] Z. Li, M. Shahidehpour, F. Aminifar, A. Alabdulwahab and Y. Al-Turki, "Networked microgrids for enhancing the power system resilience," in *Proc. IEEE*, vol. 105, no. 7, pp. 1289-1310, July 2017.
- [10] L. Liang, Y. Hou, D. J. Hill and S. Y. R. Hui, "enhancing resilience of microgrids with electric springs," *IEEE Trans. on Smart Grid*, vol. 9, no. 3, pp. 2235-2247, May 2018.
- [11] L. Che and M. Shahidehpour, "DC microgrids: economic operation and enhancement of resilience by hierarchical control," *IEEE Trans. on Smart Grid*, vol. 5, no. 5, pp. 2517-2526, Sept. 2014.
- [12] Y. Tang et al., "A review on research of cyber-attacks and defense in cyber physical power systems part two detection and protection." *Autom. Electric Power Syst.*, vol. 43, no. 10, pp. 1-9+18, 2019.
- [13] M. K. Kiptoo et al, "Integrated approach for optimal techno-economic planning for high renewable energy-based isolated microgrid considering cost of energy storage and demand response strategies," *Energy Convers. Manage.*, vol. 215, pp. 112917, 2020.
- [14] N. I. Nwulu and X. Xia, "Optimal dispatch for a microgrid incorporating renewables and demand response," *Renew. Energy*, vol. 101, pp. 16-28, 2017
- [15] R. Atia and N. Yamada, "Sizing and analysis of renewable energy and battery systems in residential microgrids," *IEEE Trans. on Smart Grid*, vol. 7, no. 3, pp. 1204-1213, May 2016.
- [16] S. Swamina, G. S. Pavlak, and J. Freihaut, "Sizing and dispatch of an islanded microgrid with energy flexible buildings," *Appl. Energy*, vol. 276, pp. 115355, 2020.
- [17] J. Zhou et al., "Economic and resilience benefit analysis of incorporating battery storage to photovoltaic array generation," *Renew. energy*, vol. 135, pp. 652-662, 2019.
- [18] M. Ahmadi, M. E. Lotfy, R. Shigenobu, A. M. Howlader and T. Senjyu, "Optimal sizing of multiple renewable energy resources and PV inverter reactive power control encompassing environmental, technical, and economic issues," *IEEE Syst. J.*, vol. 13, no. 3, pp. 3026-3037, Sept. 2019.
- [19] P. Nagapurkar and J. Smith, "Techno-economic optimization and environmental life cycle assessment of microgrids located in the US using genetic algorithm," *Energy Convers. Manage.*, vol. 181, pp. 272-291, 2019.
- [20] S. Tsianikas et al., "Economic trends and comparisons for optimizing grid-outage resilient photovoltaic and battery systems," *Appl. Energy*, vol. 256, pp. 113892, 2019.
- [21] Nicholas D. Laws et al., "Impacts of valuing resilience on cost-optimal PV and storage systems for commercial buildings," *Renew. Energy*, vol. 127, pp. 896-909, 2018.
- [22] E. Rosales-Asensio et al., "Microgrids with energy storage systems as a means to increase power resilience: An application to office buildings," *Energy*, vol. 172, pp. 1005-1015, 2019.
- [23] K. Anderson et al., "Quantifying and monetizing renewable energy resiliency," Sustainability, vol. 10, no. 4, pp. 933, 2018.
- [24] ACTIONPOWER, "Remote aircraft power supply solution," 2020. [Online]. http://www.cnaction.com/CivilGPDDetail\_2727.html
- [25] Y. Xiang, et al., "Techno-economic design of energy systems for airport electrification: A hydrogen-solar-storage integrated microgrid solution," Appl. Energy, vol. 283, pp. 116374, 2021.
- [26] J. Yu et al., "Day-ahead scheduling method of power-to-gas system considering operation characteristics of water electrolysis and methanation," *Autom. Electric Power Syst.*, vol. 43, no. 18, pp. 18-25, 2019.
- [27] Y. Zhang and W. Wei, "Model construction and energy management system of lithium battery, PV generator, hydrogen production unit and fuel cell in islanded AC microgrid," *Int. J. Hydrogen Energy*, vol. 45, no. 33, pp. 16381-16397, 2020.
- [28] L. Xu, X. Ruan, C. Mao, B. Zhang and Y. Luo, "An improved optimal sizing method for wind-solar-battery hybrid power system," *IEEE Trans. Sustain. Energy*, vol. 4, no. 3, pp. 774-785, July 2013,
- [29] Y. Xiang et al., "Cost-benefit analysis of integrated energy system planning considering demand response," *Energy*, vol. 192, pp. 116632, 2020
- [30] K. Gulan, E. Cotilla-Sanchez and Y. Cao, "Charging analysis of ground support vehicles in an electrified airport," in 2019 IEEE Trans. Electrification Conference and Expo (ITEC), 2019, pp. 1-6.



**Huangjiang Zhao** received the B.S. degree in electrical engineering and automation from the Harbin University of Science and Technology, Harbin, China, 2015. He is currently working toward the M.S. degree in electrical engineering with Sichuan University, Chengdu, China. His research interests include resilient multi energy systems, electric vehicle integration, and smart grids.



Yue Xiang (Senior Member, IEEE) received the B.S. and Ph.D. degrees from Sichuan University, Chengdu, China, in 2010 and 2016, respectively. He was a Joint Ph.D. Student with the Department of Electrical Engineering and Computer Science, University of Tennessee, Knoxville, TN, USA, from 2013 to 2014. He was a Visiting Researcher with the Department of Electrical and Electronic Engineering, Imperial College London, London, U.K., from 2019 to 2020. He is currently an Associate Professor with the College of Electrical Engineering, Sichuan University, Sichuan, China. His main research interests are distribution network planning and optimal operation, electric vehicle integration, integrated energy system planning, and smart grids.



**Yichen Shen** received the B.Eng. degrees in Electrical and Electronic Engineering from the University of Bath, U.K., and in Electrical Power Engineering from North China Electric Power University, China, both in 2017. Then, he received the Ph.D degree from the University of Bath, U.K. His research interest is resilient multi energy systems.



Yongtao Guo received the B.S. degree in electrical engineering from Guangxi University, Nanning, China, 2020. He is currently working toward the M.S. degree in electrical engineering with Sichuan University, Chengdu, China. His research interests include optimal operation and planning of integrated energy systems.



Ping Xue received the B.S. degree in electrical engineering and automation from Sichuan University, Chengdu, China, in 2019. She is currently working toward the M.S degree in electrical engineering with Sichuan University. Her research interests include distribution network planning and optimal operation, electric vehicle integration, and smart grids.



Wei Sun (Member, IEEE) received the Ph.D. degree in power system engineering from The University of Edinburgh, U.K. He is currently a Research Associate on multi-vector energy systems with The University of Edinburgh. His research interests include the development and application of optimization methods to the planning and design and operation of smart energy systems.



Hanhu Cai received the B.S. degree in electrical engineering and intelligent control from North University of China, Taiyuan, China, in 2017 and the M.S. degree in electrical engineering from the Sichuan University, Chengdu, China, in 2021. He is currently working at the Southwest Electric Power Design Institute CO., LTD. of China Power Engineering Consulting Group, Chengdu, China. His main research interests are integrated energy system planning, optimal operation and economic analysis.



Chenghong Gu (Member, IEEE) received the master's degree in electrical engineering from Shanghai Jiao Tong University, Shanghai, China, in 2007, and the Ph.D. degree in electrical engineering from the University of Bath, Bath, U.K., in 2010. He is currently a Lecturer and EPSRC Fellow with the Department of Electronic and Electrical Engineering, University of Bath. His research interests include multi-vector energy system, smart grid, and power economics.



**Junyong Liu** (Member, IEEE) received the Ph.D. degree in electrical engineering from Brunel University, London, U.K., in 1998. He is currently a Professor with the College of Electrical Engineering, Sichuan University, Chengdu, China. His research interests include power system planning, operation, and electricity marking.